Journal of Membrane Science 712 (2024) 123240

Contents lists available at ScienceDirect

Journal of Membrane Science

journal homepage: www.elsevier.com/locate/memsci

A cationic three-dimensional covalent organic framework membrane for nanofiltration of molecules and rare Earth ions

Xiansong Shi [a], Xingyuan Wang [a], Tianci Feng [a], Tong Ju [a], Jianghai Long [a], Congcong Yin [b], Zhe Zhang [c], Yong Wang [a,b,*]

[a] State Key Laboratory of Materials-Oriented Chemical Engineering, College of Chemical Engineering, Nanjing Tech University, Nanjing, 211816, Jiangsu, PR China
[b] School of Energy and Environment, Southeast University, Nanjing, 210096, Jiangsu, PR China
[c] School of Environmental Science and Engineering, Nanjing Tech University, Nanjing, 211816, Jiangsu, PR China

ARTICLE INFO

Keywords:
3D COFs
Membrane
Molecular separation
Ion sieving
Rare earth elements

ABSTRACT

Permanently microporous materials have evolved as focal point of research for tackling issues in separation science and membrane technology. Covalent organic frameworks (COFs) stand out for their distinctive synergy of crystalline nature, uniform channels, and structural diversities. Three-dimensional (3D) COFs, distinguished by angstrom-sized and interconnected channels, hold special promise for separating small targets; however, this potential remains underexplored. Here, we report feasible growth of cationic 3D COF membranes on a flexible polymer substrate for versatile nanofiltration toward both molecules and ions. Through comprehensive performance evaluations, we reveal that the resultant membrane exhibits durable and prominent molecular selectivity to separate fine species with molecular weights above 300 g mol^{-1} at fast methanol permeation. Lanthanide ions of industrial value also can be harvested by the membrane with rejection rates of up to 91.4%. Together with its nonselectivity to competing ions, our membrane implements efficient extraction of rare earth elements from ion mixtures. These findings illuminate the potential of 3D COFs for liquid separation and offer a solution to building versatile membranes.

1. Introduction

Separating industrially valued substances in liquids represents a ubiquitous necessity of paramount significance in chemical separation across diverse high-tech fields [1]. As exemplified by pharmaceutical refinement, the separation process is pivotal in determining the quality and efficacy of the final products. Similarly, size-dispersive raw nanomaterials, such as quantum dots, require precise fractionation to exert their size-dependent photoelectric capability [2]. Besides molecules and nanoparticles, ionic objects, with attractive industrial potential toward energy, aviation, and therapy, are experiencing rapidly growing demand [3,4]. There is a global strategic focus on extracting precious metal ions, such as rare earth elements known for their special electronic features, from mineral deposits [5]. These desired species often coexist with substantial impurities, posing a challenge to their selective extraction and purification. While conventional strategies like solvent extraction and chromatography have been utilized, the tedious and energy-intensive procedures limit their cost-effectiveness. Selective adsorbents are developed as a versatile and efficient alternative to enriching targeted molecules and ions [6,7]. However, the problems of absorbent regeneration, limited productivity, and considerable footprint turn out to be potential barriers that likely hinder industrial realization.

Liquid-phase membrane technology, inclusive of reverse osmosis, nanofiltration, and ultrafiltration, is deemed as an eco-friendly and energy-efficient option for separating solutes from solvents [8–10]. Among these techniques, nanofiltration stands out for its unique synergy of low operating pressures, high selectivity, and versatility [11]. Through rational design of the pore microenvironments in nanofiltration membranes, their separation accuracy can be fine-tuned to discriminate mixtures of molecules and/or ions [12]. This broad spectrum of separation capabilities makes nanofiltration protocol appealing for recovering and purifying value-added targets like rare earth elements. The overall performance of nanofiltration membranes stems from the structure and properties of their constituent materials [13]. Research efforts have thus been focused on exploring viable materials, including polyamide and its derivatives, ultrathin nanosheets, and microporous

* Corresponding author. State Key Laboratory of Materials-Oriented Chemical Engineering, College of Chemical Engineering, Nanjing Tech University, Nanjing, 211816, Jiangsu, PR China; School of Energy and Environment, Southeast University, Nanjing, 210096, Jiangsu, PR China.
E-mail address: yongwang@seu.edu.cn (Y. Wang).

https://doi.org/10.1016/j.memsci.2024.123240
Received 10 July 2024; Received in revised form 20 August 2024; Accepted 21 August 2024
Available online 23 August 2024

polymers, for constructing nanofiltration membranes with optimized performance [14–17]. Many of these membranes, however, may abide by permeance-selectivity trade-offs, deficient separation precision, and compromised performance over prolonged operation periods. Therefore, developing game-changing materials capable of nanofiltration with improved performance and durability is an urgent priority.

Covalent organic frameworks (COFs) built through the reticular chemistry represent a vast family of extended porous crystalline materials with broad structural and chemical diversities [18–21]. Their regularly arranged uniform pores can act as a mass transport highway to permit fast solvent permeation with desired solute-solute selectivity [22]. Well-crystallized skeletons and strong covalent connections between organic precursors endow COFs with eminent physicochemical durability to resist performance compromise even after long-term use [23]. This evolving material therefore stands at the forefront of developing next-generation membranes with better-performing selectivity and stability [24–26]. Thus far, COFs featuring topologically designed two-dimensional (2D) and three-dimensional (3D) motifs have been grown into continuous membranes to tackle unresolved issues in separation science [27,28]. The groundbreaking studies reported by Banerjee et al. took the lead in crystallizing COF membranes and in exposing their possibility for liquid separation [29,30]. Jiang et al. leveraged the function design of COFs to yield high-selectivity membranes for ion sieving [31,32]. Fan and co-workers proposed diverse innovative methodologies to structurally devise COF membranes with improved gas separation performance [33,34]. In the past decade, membranes constructed by 2D COFs with unique straight channels has been the focus in this field, possibly due to their numerous membrane-forming methods, such as solvothermal growth, nanosheet assembly, and interfacial crystallization [35]. However, the large aperture size of 2D COFs, mostly in the range of 1–5 nm, hampers their efficacy in separating ultrafine species with close sizes and properties. By comparison, the spatial interpenetration of 3D COFs gives rise to narrowed channels that could meet ever-growing membrane selectivity. Besides, unlike the mutually disjoint pores of 2D COFs, the channels of 3D COFs feature desired dimensional interconnectivity, providing abundant accessible pathways to facilitate mass transport. Despite these benefits, the proportion of 3D COF membranes among COF-based membranes reported so far remains extremely low (<5%), resulting in a scarce insight into the full potential of 3D COFs as membrane materials [32,36–38]. Moreover, developing separation membranes based on 3D COFs, especially those with intrinsically charged backbones, continues to present intractable challenges because of their structural characteristics.

Here, we present facile solvothermal growth of a cationic 3D COF on a mesoporous polyimide substrate to produce a versatile membrane for size-dependent nanofiltration of both molecules and rare earth ions. The chemically crosslinked polyimide substrate affords an active surface for crystallizing continuous 3D COF membranes with a compact structure. We discover that the synthetic membrane can function as a molecular sieving gate to separate fine molecular pairs while allowing for fast solvent permeation. In addition, analyses of the membrane performance in rare earth element extraction reveal its competence to selectively harvest lanthanide ions from a complex system enriched with competing ions. The realization of 3D COF membranes here provides an avenue to build versatile membranes capable of meeting multiple separation demands.

2. Experimental section

2.1. Materials

Tetrakis(4-formylphenyl)-methane (TFPM, 99%) was obtained from Jilin Chinese Academy of Sciences-Yanshen Technology. Ethidium bromide (EB, 98%), isopropanol (AR), tetracycline (CP), rifampicin (98%), bacitracin (>60 units mg^{-1}), methyl-2-pyrrolidinone (NMP, 99%), lanthanum nitrate ($La(NO_3)_3$, 99.9%), neodymium nitrate ($Nd(NO_3)_3$, 99.9%), europium nitrate ($Eu(NO_3)_3$, 99.99%), ytterbium nitrate ($Yb(NO_3)_3$, 99.99%), lanthanum chloride ($LaCl_3$, 99.9%), and strontium chloride ($SrCl_2$, 99.9%) were obtained from Macklin. Amoxicillin (99%), spiramycin (90%), potassium bromide (KBr, 99%), scandium(III) triflate ($Sc(OTf)_3$, 98%), *n*-propanol (99.5%), and caesium chloride (CsCl, 99.9%) were purchased from Aladdin. Ethanol (99.7%) and vitamin B12 (VB-12) were obtained from Sinopharm Chemical Reagent and J&K Chemical, respectively. Methyl orange (MO), Congo red (CR), Evans blue (EvB), chrome black T (CB-T), *p*-nitrophenol (NP, 99%), acid fuchsin (AF), and dioxane (98%) were supplied by the Institute of Chemical Reagent. Paracetamol (98%) was obtained from Tianjin Heowns Biochemical Technology. Methanol (99.5%) and *n*-butanol (99%) were supplied by Shanghai Lingfeng Chemical Reagent and Shanghai Shenbo Chemical, respectively. Polyimide (PI) particles (P84) were provided by HP Polymer GmbH (Austria). Other reagents including hexamethylenediamine (HDA, 99%) and polyethylene glycol (M_w = 400 g mol^{-1}, PEG400, 99%) were obtained from local suppliers and used as received. Deionized (DI) water (conductivity = 2–10 μS cm^{-1}) was utilized throughout this study.

2.2. Solvothermal synthesis of TFPM-EB powders

TFPM (0.05 mmol, 21.6 mg) and EB (0.1 mmol, 39.3 mg) was charged into a Pyrex tube, followed by the addition of a mixed solution containing 1,4-dioxane (1.0 mL) and acetic acid (3 mol L^{-1}, 0.1 mL). The obtained mixture was sonicated to achieve sufficient dispersion. Afterwards, the tube was flash-frozen in a liquid N_2 bath and subjected to three freeze-pump-thaw cycles for degassing. The tube was flame-sealed and treated at 85 °C for 72 h. The resulting precipitates were thoroughly washed with tetrahydrofuran and finally dried at 85 °C overnight.

2.3. Preparation of CPI substrates

PI substrates were fabricated by a nonsolvent induced phase separation method. PI solids were first vacuum-dried at 80 °C for 12 h and added to a mixture of NMP (solvent) and PEG400 (porogen) to form a polymer dope. The mass concentrations of PI, PEG400, and NMP were 20, 5 and 75 wt%, respectively. The dope was rigorously stirred at 80 °C for 5 h and kept undisturbed at room temperature for at least 24 h to generate a homogeneous solution. The solution was cast on a non-woven fabric through a blade with a gap of 200 μm, which was immersed into DI water. The obtained PI substrates were successively washed with DI water and isopropanol, which were then immersed in a solution comprising of 5 wt% HDA in isopropanol for 24 h at room temperature to generate solvent-resistant crosslinked PI (CPI) substrates. After crosslinking, the CPI substrates were washed with isopropanol to eliminate the residual HDA and kept in isopropanol before use.

2.4. Synthesis of TFPM-EB membranes

TFPM-EB selective layers were grown on the CPI substrate under solvothermal conditions to generate composite membranes. TFPM (0.025 mmol, 10.8 mg), EB (0.05 mmol, 19.7 mg), and $Sc(OTf)_3$ (5–20 mg) were charged into a 100-mL Teflon lining, followed by the addition of 1,4-dioxane (25 mL). The solution was ultrasonicated to obtain sufficient dispersion. Afterwards, three pieces of CPI substrates were loaded in a home-made nylon holder, and then the holder was transferred into the lining. The lining was sealed into a stainless-steel reaction autoclave and heated at 85 °C. After designated durations, the TFPM-EB composite membranes were washed with ethanol and stored in ethanol before further tests.

2.5. Characterizations

Surface topography of the membranes was tested through atomic force microscopy (AFM, XE-100, Park Systems). Scanning electron

microscopy (SEM, Hitachi S-4800) tests of the TFPM-EB powders and membranes were carried out at an accelerating voltage of 3 kV. Fourier transform infrared (FTIR, Nicolet 8700) spectroscopy tests were conducted on the monomers, TFPM-EB powders, and membranes with the wavenumber in the range of 4000–400 cm^{-1}. KBr pellet and attenuated total reflection methods were utilized for powder and membrane tests, respectively. Transmission electron microscopy (TEM) tests were performed on an FEI Talos F200X G2 microscope at 200 kV. Surface Zeta potentials were conducted on a SurPass electrokinetic analyser (Anton Paar GmbH). Elemental analysis was performed through energy dispersive X-ray (EDX) mapping. Powder X-ray diffraction (PXRD) patterns of TFPM-EB powders were recorded by a Rigaku Smart Lab X-ray diffractometer with Cu Kα radiation (λ = 0.15418 nm) at 2θ of 2–40°. Nitrogen adsorption-desorption tests were performed on a surface area and porosity analyser (Micrometrics ASAP2460) at 77 K. Brunauer-Emmett-Teller (BET) surface areas and pore size distributions were generated from the adsorption curves based on the non-local density functional theory. Surface contact angles were measured through a contact angle goniometer (DropMeter A100, Maist). A nanoindentation instrument (Agilent, Nano Indenter G200) was used to determine the mechanical strength of the TFPM-EB membrane.

2.6. Filtration tests

Organic solvent nanofiltration and rare earth element recovery performance of the TFPM-EB membranes were assessed at a transmembrane pressure (P) of 1 bar by an Amicon 8003 filtration cell (Millipore). Membrane permeance (P, L m^{-2} h^{-1} bar^{-1}) was obtained as follows:

$$P = V/(AtP) \quad (1)$$

where V (L) is the permeated solvent volume, A (m^2) is the effective membrane area, t (h) is the tested duration. Separation performance was explored using 10-ppm dye methanolic solutions or 1000 ppm salt aqueous solutions as feed. The structures of the used dye molecules were optimized using ChemDraw and then their sizes were estimated using Materials Studio. The rejection rate (R, %) was obtained as follows:

$$R = \left(1 - C_p / C_f\right) \times 100\% \quad (2)$$

where C_f and C_p represent the concentrations of the probe species in the feed and permeate, respectively. For dyes in methanol, their concentrations were determined using a NanoDrop 2000C UV–vis spectrophotometer (Thermo Fisher); for single-component salts in water, their concentrations were measured using an electrical conductivity meter (S230–K, Mettler-Toledo); for trinary-component salts in water, their concentrations were tested through inductively coupled plasma optical emission spectrometry (PerkinElmer Optima 7000 DV). The ion selectivity (S) toward ion a and ion b was calculated based on their rejections (R_a and R_b) as follows:

$$S = (1 - R_b) / (1 - R_a) \quad (3)$$

3. Results and discussion

Fig. 1a diagrammatizes the diameters of the hydrated ions [39]. To achieve the selective separation of La^{3+}, the membrane material should afford a narrowed pore size distribution with an effectual sieving pore size within ~0.8–0.9 nm. Thus, TFPM-EB, built from the Schiff-base reaction between tetrahedral aldehyde TFPM and electropositive amine EB [40], was selected as the representative 3D ionic COF (Fig. 1b). We studied the structure of the TFPM-EB powder synthesized through a solvothermal method. As shown in Fig. 1c, FTIR spectra detect

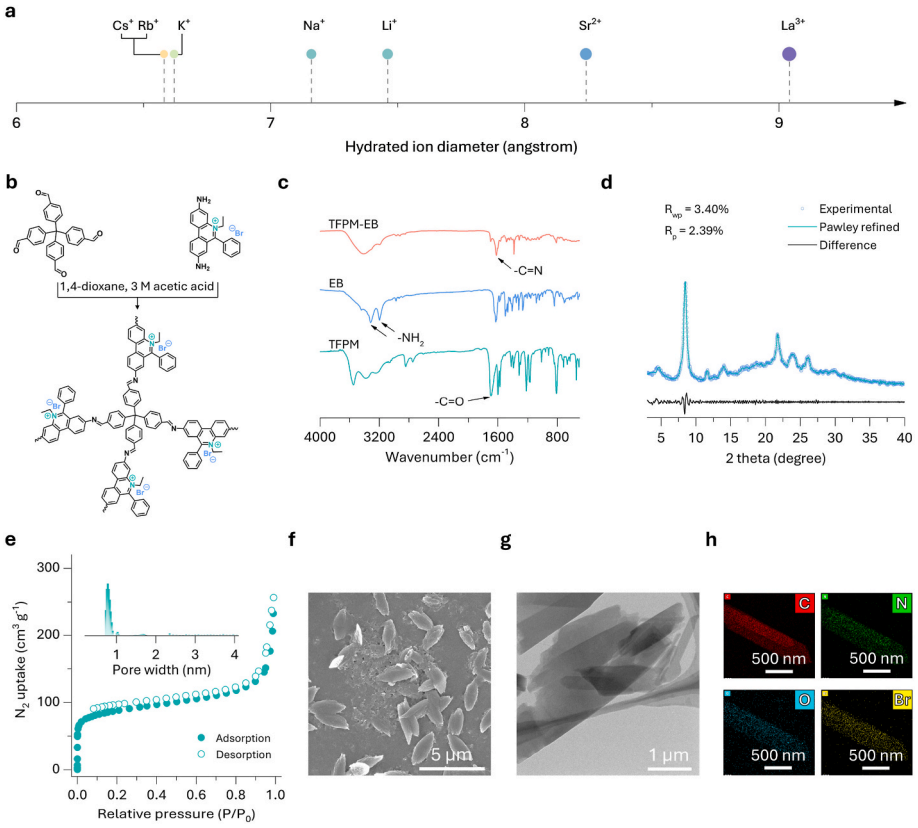

Fig. 1. Preparation and characterization of TFPM-EB. (a) Diameters of the hydrated ions. (b) Schematic preparation of TFPM-EB. (c) FTIR spectra of TFPM-EB, EB, and TFPM. (d) PXRD patterns of the TFPM-EB powder with the experimental, refined, and difference profiles. (e) N_2 sorption isotherms at 77 K. (f) SEM, (g) TEM, and (h) EDX images of the TFPM-EB powder. Inset in (e) shows the pore width distribution.

the absence of –C═O (~1686 cm^{-1}) from TFPM and N–H (~3195 cm^{-1} and ~3316 cm^{-1}) from EB, which validates the condensation between the building units. The stretching vibration of –C═N (~1622 cm^{-1}) in the FTIR spectrum of TFPM-EB elucidates its imine-linked structure [41]. Pawley refinement was conducted based on the experimental PXRD pattern and the 3-fold interpenetrated *dia* topology previously reported [40]. The tetragonal unit cell parameters of a = b = 37.74 Å, c = 14.82 Å, and α = β = γ = 90° are deduced for TFPM-EB and the sharp diffraction peak at ~8.5° corresponds to the (121) crystal facet, confirming its high crystallinity (Fig. 1d). The N_2 sorption measurement verifies a well-defined microporous structure of TFPM-EB, with a narrow pore width distribution ranging from 0.7 to 0.86 nm (Fig. 1e). This angstrom-scale channels with spatially interconnected porosity could promise the expected membrane selectivity with minimal compromise in permeance. SEM and TEM tests reveal a rod-like structure of TFPM-EB (Fig. 1f–g, Fig. S1). The EDX images visualize a homogeneous distribution of the key elements, namely C, N, O, and Br, throughout TFPM-EB (Fig. 1h), aligning with its chemical composition.

Having examined the microporosity and morphology of TFPM-EB, we turned to producing its membrane for separation application. TFPM-EB was crystallized on a CPI substrate through solvothermal growth with the catalysis of $Sc(OTf)_3$, as illustrated in Fig. 2a. With the crosslinking of HDA, the linear polyimide polymers can be weaved into three-dimensionally interlaced networks (Fig. S2). The crosslinked

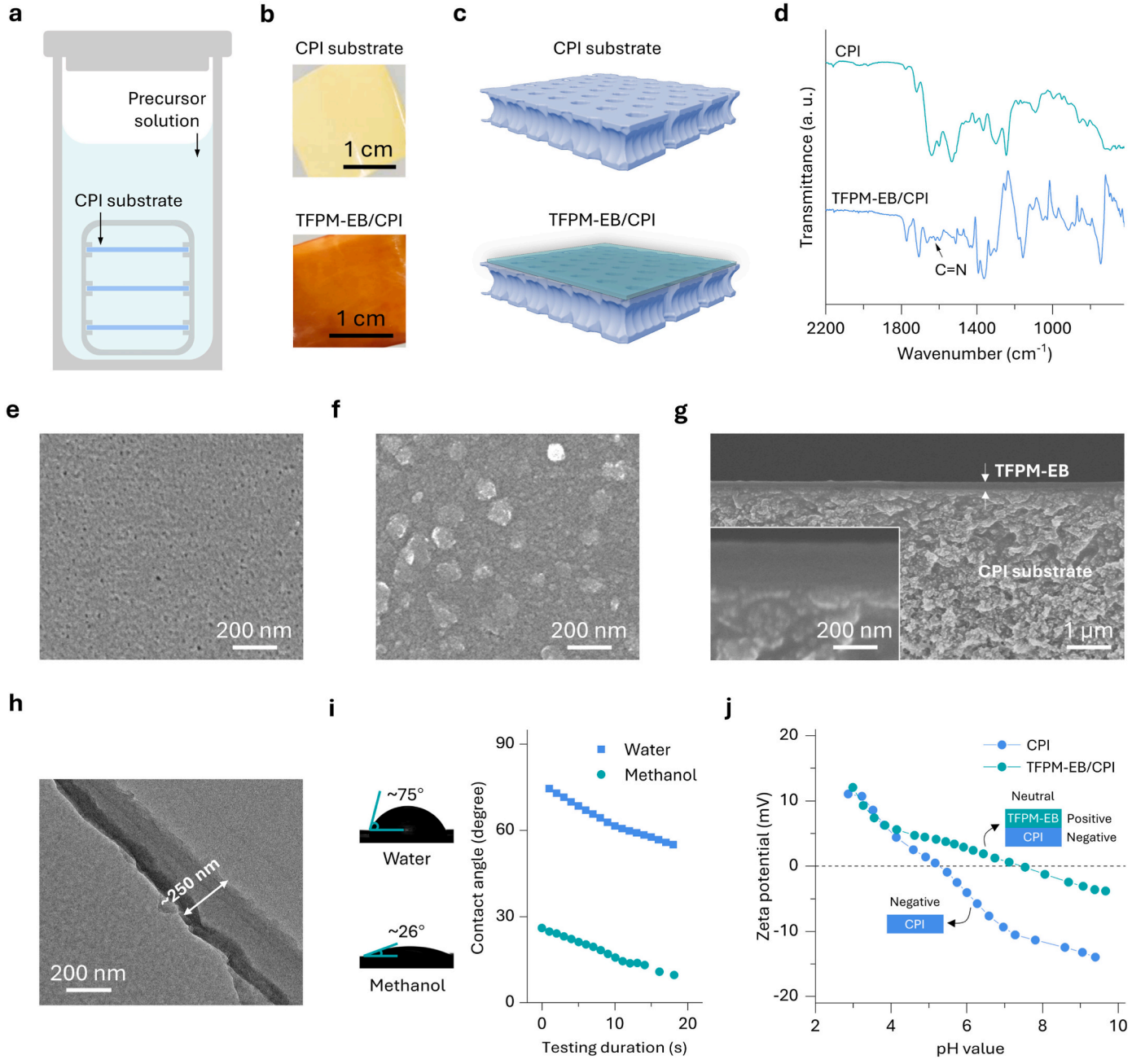

Fig. 2. Preparation and characterization of TFPM-EB membranes. (a) Schematic representation for the growth of TFPM-EB membranes. (b) Photographs of the CPI substrate and TFPM-EB/CPI membrane. (c) Schematic illustration of the CPI substrate and TFPM-EB/CPI membrane. (d) FTIR spectra of the CPI substrate and TFPM-EB/CPI membrane. (e) Surface SEM image of the CPI substrate. (f) Surface SEM, (g) cross-sectional SEM, and (h) cross-sectional TEM images of the TFPM-EB/CPI membrane. (i) Water and methanol contact angles of the TFPM-EB/CPI membrane. (j) Zeta potential profiles of the CPI substrate and TFPM-EB/CPI membrane. Inset in (g) shows the magnified cross-sectional SEM image of the TFPM-EB membrane.

polyimide offers excellent chemical stability for growing membranes [42], as confirmed by the intact porous structure after being treated with the solvothermal conditions (Fig. S3). Moreover, the terminal amine groups of HDA on substrate can function as nucleation sites to promote the growth of defect-free TFPM-EB layers. The contrast on the FTIR spectra of the neat and crosslinked polyimide membranes reveals the conversion of labile polyimide to robust polyamide networks (Fig. S4) [37]. After solvothermal growth, we notice a distinct surface colour change from yellow to brown (Fig. 2b), indicating the growth of TPFM-EB. The synthesis of TFPM-EB on the top of CPI substrate thus generates a composite membrane, as shown in Fig. 2c. The emergence of typical stretching vibrations at 1620 cm^{-1} confirms the existence of imine-linked frameworks (Fig. 2d). SEM imaging of the substrate surface reveals that its mesoporous structure keeps intact after being chemically crosslinked (Fig. 2e, Fig. S5). The growth of TFPM-EB is demonstrated to have a profound dependence on the synthesis time. Prolonging the

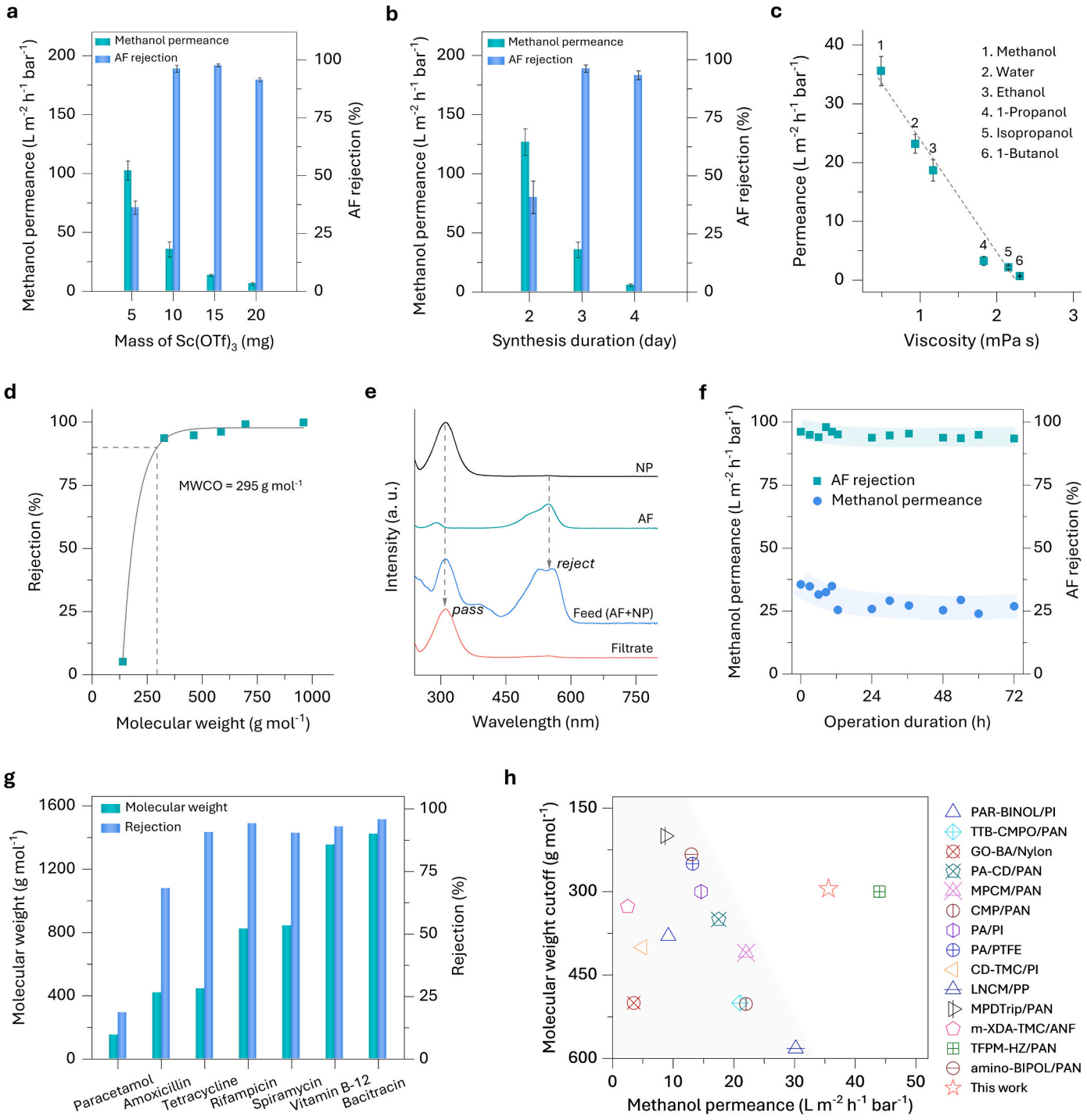

Fig. 3. Molecular separation of TFPM-EB membranes. (a) Methanol permeance and AF rejection of the TFPM-EB/CPI membranes synthesized with various amounts of $Sc(OTf)_3$. (b) Methanol permeance and AF rejection of the TFPM-EB/CPI membranes synthesized with various durations. (c) Pure solvent permeance of the TFPM-EB/CPI membrane as a function of solvent viscosity. (d) Molecular rejection curve of the TFPM-EB/CPI membrane. (e) UV–vis spectra for the molecular sieving of the NP/AF mixture. (f) Performance of the TFPM-EB/CPI membrane as a function of operation duration. (g) Rejection of various pharmaceuticals. (h) Performance comparison between the TFPM-EB/CPI membrane and the state-of-the-art membranes.

synthesis time conduces to producing dense and compact TFPM-EB membranes (Fig. S6). A synthesis duration of 3 days generates a composite membrane with continuous TFPM-EB that can serve as the selective layer for separation (Fig. 2f). The cross-sectional SEM observation shows a uniform TFPM-EB separation layer firmly adhered to the CPI substrate (Fig. 2g). TEM imaging and EDX analyses of the cross-sectional membrane slice reveal a nanoscale TFPM-EB thickness of ~250 nm (Fig. 2h, Fig. S7). Tight stacking of TFPM-EB crystals without grain boundary gaps is recognized by AFM imaging (Fig. S8). In addition, the nanoindentation test shows that the TFPM-EB membrane has reduced modulus (E) and hardness (H) values of 2.8 and 0.4 GPa, respectively (Fig. S9), suggesting notable mechanical strength [43,44]. The resultant membrane shows mediocre hydrophilicity due to the aromatic framework of TFPM-EB, while it presents a high affinity with methanol (Fig. 2i). This structural nature could promise rapid permeation of organic liquids. The Zeta potential measurement of the CPI substrate determines a negatively charged surface (Fig. 2j). With the covering of cationic TFPM-EB, the surface charge is substantially neutralized for the composite membrane. As a result, the surface Zeta potential is tested to be ~0.7 mV at a pH value of 7.1, identifying a nearly neutral surface free of charge-dependent repulsion in separation [45].

We evaluated the molecular separation ability of TFPM-EB membranes synthesized under different conditions to determine their separation performance. Fig. 3a depicts methanol permeance and AF (molecular weight = 585.5 g mol^{-1}) rejection of the membranes crystallized from various amounts of $Sc(OTf)_3$ for 3 days. The result shows that the methanol permeance decreases with the increase of $Sc(OTf)_3$ amount, while the AF rejection is largely improved. This is related to the fact that the growth of TFPM-EB becomes intensified with higher catalyst amounts. Adding 10 mg of $Sc(OTf)_3$ generates a membrane with methanol permeance of 35.6 L m^{-2} h^{-1} bar^{-1} and AF rejection as high as 96.2%. Apart from the amount of $Sc(OTf)_3$, the performance of TFPM-EB membranes is also dictated by the growth time. A synthesis period of 3 days can produce the membrane with maximized performance (Fig. 3b). Permeation behaviour of various solvents was studied to understand the solvent transport mechanism in our membrane. When correlating the permeances with solvent parameters including Hansen solubility parameter, viscosity, and kinetic diameter, it shows that the solvent permeances display an approximately linear relationship with solvent viscosity (Fig. 3c, Fig. S10), following the Hagen-Poiseuille equation [46,47]. The membrane was challenged with a range of small molecules dissolved in methanol to investigate its selectivity (Fig. S11). A sharp rejection curve with a low molecular weight cutoff (MWCO) of ~295 g mol^{-1} manifests high membrane selectivity (Fig. 3d, Fig. S12). By virtue of this prominent selectivity, our membrane achieves selective sieving of a molecular mixture composed of AF and NP (molecular weight = 139.1 g mol^{-1}). As depicted in Fig. 3e, the characteristic peak belonging to NP at 311 nm remains in the filtrate spectrum, while the AF peak at 548 nm disappears. This indicates effectual molecular sieving through the membrane, with NP and AF rejection rates of 24.7% and 97.1%, respectively. The slight difference in their rejection rates toward single- and bi-component systems may arise from solute-solute interactions in the bi-component system. Given the uncharged membrane surface and the separation in nonaqueous liquid, the size-based exclusion is believed to be decisive in this molecular sieving process [48]. The membrane further demonstrates stable performance without significant compromise in a prolonged testing period of 72 h (Fig. 3f). The stability in terms of crystallinity could be responsible for this performance durability (Fig. S13). In addition to the dye rejection, the synthesized membrane was also applicable to concentrate pharmaceuticals of biomedical values. The result shows that our membrane can effectively separate pharmaceuticals with molecular weights above 440 g mol^{-1} (Fig. 3g), indicating its practicality toward pharmaceutical industry [49]. We diagrammatized the performance of the state-of-the-art membranes and our membrane (Fig. 3h–Table S1). Clearly, the TFPM-EB membrane in this work permits fast methanol permeation and accurate molecular separation performance, highlighting its superiority to implement molecular separation in organic liquids [50].

In light of the prominent molecular selectivity, we were dedicated to exploring the applicability of the membrane developed here in the separation of rare earth elements, which hold indispensable roles in a multitude of applications [51]. $La(NO_3)_3$ dissolved in water with a concentration of 1000 ppm was used as a typical target to explore rare earth ion separation performance of our membranes. It should be noted that the CPI substrate shows water permeance of 850 L m^{-2} h^{-1} bar^{-1} and inappreciable $La(NO_3)_3$ rejection of below 10%, indicating that the substrate contributes to ion rejection scarcely. Fig. 4a presents the water permeance and $La(NO_3)_3$ rejection of the membranes as a function of synthesis time. With the extension of synthesis duration from 24 to 96 h, the water permeance declines and the rejection rate increases continuously. The optimal synthesis time is regarded as 72 h, which can generate a potent TFPM-EB membrane that exhibits water permeance of 23.2 L m^{-2} h^{-1} bar^{-1} and high $La(NO_3)_3$ rejection of 91.4%. The membrane synthesized with 72 h was assessed to gain more insights into its competence to fulfil rare earth element separation. The membrane rejection of aqueous $La(NO_3)_3$ solutions with reduced concentrations was explored because of the low rare earth ion concentrations (one to hundreds of ppm) in real-world extraction processes [52]. Significantly, the $La(NO_3)_3$ rejection keeps above 90% as the concentration ranges from 100 to 1000 ppm (Fig. 4b), indicative of stable performance to recover La^{3+} from aqueous solution. The slightly enhanced rejection at higher concentrations could be attributed to the concentration polarization at membrane surface, which impedes the infiltration of ions to improve membrane rejection [53]. Having confirmed the satisfactory separation performance toward La^{3+}, we next evaluated the potential of the TFPM-EB membrane for recovering other rare earth ions. A series of rare earth nitrates, including $Nd(NO_3)_3$, $Eu(NO_3)_3$, and $Yb(NO_3)_3$, were selected to challenge the membrane, with rejection rates of 84.5%, 82%, and 90.3%, respectively (Fig. 4c). This finding reveals that our membrane is applicable to concentrate rare earth elements from aqueous solutions.

We examined both the mechanical and chemical stabilities of the membrane to disclose its performance robustness. In a reutilization test for 5 cycles, the membrane shows insignificant changes in both the water permeance and $La(NO_3)_3$ rejection (Fig. 4d). To be specific, the membrane still performs $La(NO_3)_3$ rejection of 88.5% together with water permeance of 20.9 L m^{-2} h^{-1} bar^{-1} after 5-cycle separation. Acidic environments are often involved in the industrial concentration and extraction of rare earth ions [54]. To integrate membrane technology with the existing industrial processes, the utilized membrane should afford decent chemical stability to resist low pH conditions. The membrane building material, TFPM-EB, was treated with a 1 mol L^{-1} HCl aqueous solution for 3 days followed by PXRD tests. The PXRD patterns in Fig. 4e illustrate that the treatment generates no significant damage to the crystallinity of TFPM-EB, as confirmed by the well-maintained diffraction peaks. Our membrane can also survive in this harsh treatment, with no obvious change of structures (Fig. 4f). More importantly, the membrane rejection to various rare earth nitrates keeps uncompromised after being treated with a 1 mol L^{-1} HCl aqueous solution for 3 days (Fig. 4g). Results of these unambiguously prove the mechanical and chemical stability of our membrane, promising for real-world rare earth mining process.

In the extraction process of rare earth elements, lanthanides often coexist with alkaline earth metals and alkaline metals in waste and natural ores, causing a problem for their selective recovery [55]. Taking the separation of La^{3+}, Sr^{2+}, and Cs^{+} as a proof-of-concept study, we explored the separation performance of our membrane toward each individual component and their tri-component mixture (Fig. 4h). In single-component separation tests, the membrane demonstrates rejection rates of 53.4% for Sr^{2+} and 2.4% for Cs^{+}, along with a substantial rejection rate for La^{3+}. As for the separation of their trinary mixture, the

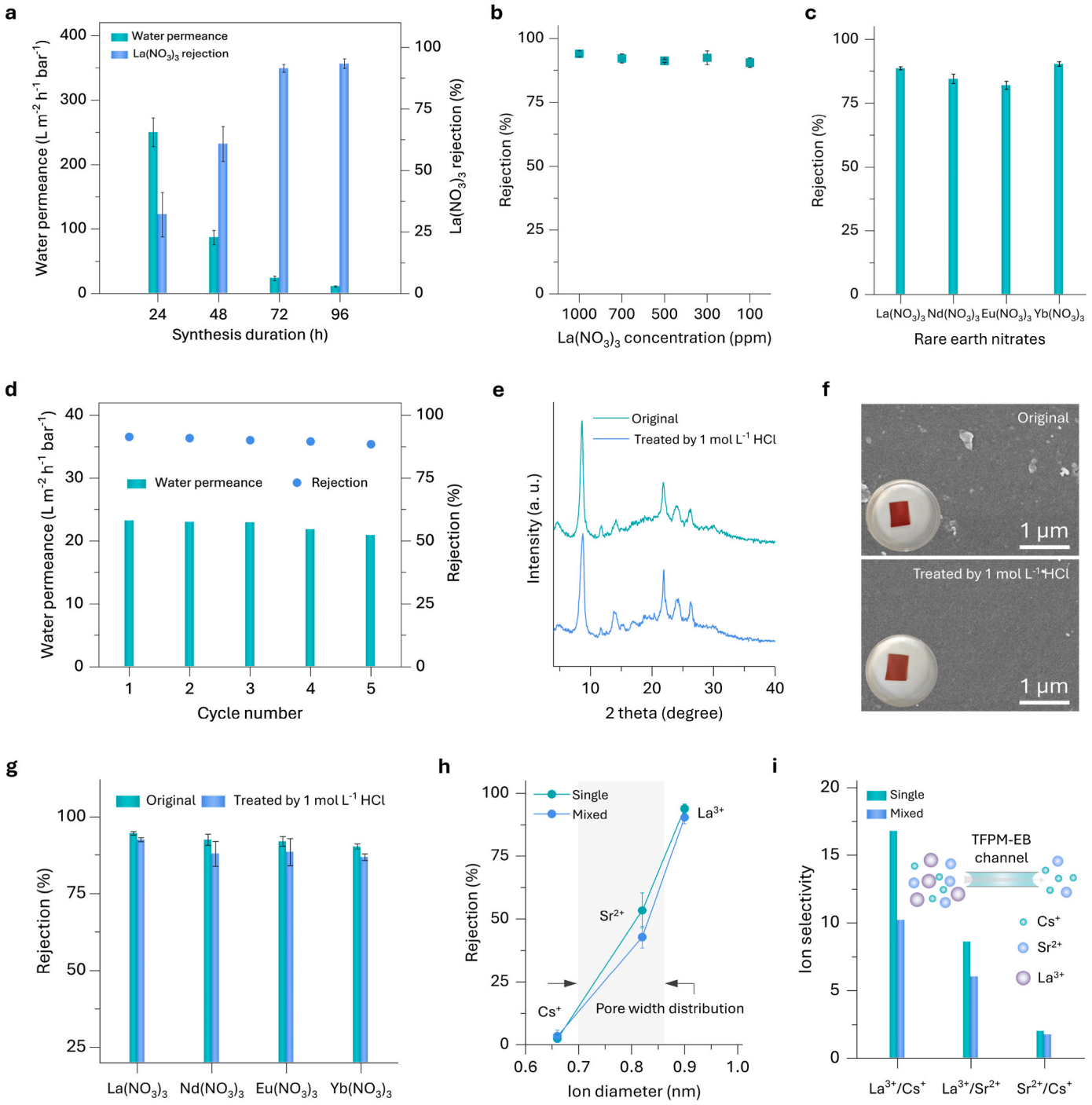

Fig. 4. Rare earth element recovery of TFPM-EB membranes. (a) Water permeance and $La(NO_3)_3$ rejection of the TFPM-EB/CPI membranes synthesized with different durations. (b) $La(NO_3)_3$ rejection of the TFPM-EB/CPI membrane as a function of $La(NO_3)_3$ concentration. (c) Rejection of the TFPM-EB/CPI membrane toward various rare earth nitrates. (d) Water permeance and $La(NO_3)_3$ rejection of the TFPM-EB/CPI membrane in 5-cycle filtration. (e) PXRD patterns of the TFPM-EB powder before and after being treated with 1 mol L^{-1} HCl for 3 days. (f) SEM images and (g) rejection of the TFPM-EB/CPI membrane before and after being treated with 1 mol L^{-1} HCl. (h) Ion rejection and (i) ion selectivity of the TFPM-EB/CPI membrane in single- and trinary-component systems. Insets in (f, i) show the photographs of the corresponding membranes and the schematic diagram of ion separation, respectively.

rejection rates of La^{3+}, Sr^{2+} and Cs^{+} are comparable to those obtained in the single-component test. To elucidate the separation mechanism, we correlated the TFPM-EB pore width distribution with the diameters of the hydrated cations used. The pore width of TFPM-EB is determined to range from 0.7 to 0.86 nm based on the analysis of the N_2 sorption isotherms. This pore width range should keep constant because of the robust structure of TFPM-EB. The diameters of the hydrated La^{3+}, Sr^{2+} and Cs^{+} are estimated to be 0.90, 0.82 and 0.66 nm, respectively [39]. In our case, the membrane largely rejects hydrated La^{3+}, while the hydrated Cs^{+}, with a size smaller than the pore width, can permeate through the membrane. Moreover, our membrane delivers moderate rejection to Sr^{2+}, whose hydrated diameter falls within the pore width range. Together with the low adsorption effect confirmed by EDX data (Fig. S14), the separation is likely dominated by size-based exclusion. The ion selectivities during the separation tests were assessed, as depicted in Fig. 4i. The ideal La^{3+}/Cs^{+} selectivity calculated from the

rejection rate of the single-component separation is 16.8, while the separation of the trinary mixture yields a high La^{3+}/Cs^{+} selectivity of 10.2. When compared with the ideal ion selectivity, the membrane selectivity toward a tri-component system is compromised, possibly due to the ion competitive effect induced by concentration polarization [56]. Overall, the membrane separation method presented here holds promise as a pretreatment step to promote the efficiency of lanthanide mining.

4. Conclusions

To conclude, our work presents facile solvothermal growth of 3D COFs on a chemically crosslinked polyimide substrate to yield robust composite membranes for separating small targets through size-dependent nanofiltration. This offers a viable platform for engineering a versatile membrane that permits selective separation of molecules and efficient extraction of rare earth elements concurrently. In particular, the resulting membrane performs an exceptional sieving ability to discriminate bi-component molecules with molecular weights of 139.1 and 585.5 g mol^{-1}. In addition, our membrane delivers the selective extraction of lanthanide ions from their competing ions, with an experimental La^{3+}/Cs^{+} selectivity of up to10.2 in a tri-component system. Overall, this research underscores the potency of 3D COFs for both molecular and ionic nanofiltration and expands access to versatile membranes for multifarious separations.

CRediT authorship contribution statement

Xiansong Shi: Writing – review & editing, Writing – original draft, Methodology, Data curation, Conceptualization. **Xingyuan Wang:** Writing – review & editing, Writing – original draft, Validation, Investigation, Data curation. **Tianci Feng:** Methodology, Investigation. **Tong Ju:** Methodology, Investigation. **Jianghai Long:** Methodology, Investigation. **Congcong Yin:** Writing – review & editing, Investigation. **Zhe Zhang:** Writing – review & editing, Methodology, Funding acquisition. **Yong Wang:** Writing – review & editing, Supervision, Funding acquisition, Conceptualization.

Declaration of competing interest

The authors declare that they have no known competing financial interests or personal relationships that could have appeared to influence the work reported in this paper.

Data availability

Data will be made available on request.

Acknowledgements

This work was supported by the National Key Research and Development Program of China (2022YFB3805201) and the National Natural Science Foundation of China (22308147, 21921006).

Appendix A. Supplementary data

Supplementary data to this article can be found online at https://doi.org/10.1016/j.memsci.2024.123240.

References

[1] D.S. Sholl, R.P. Lively, Seven chemical separations to change the world, Nature 532 (2016) 435–437.
[2] I. Moreels, K. Lambert, D. Smeets, D. De Muynck, T. Nollet, J.C. Martins, F. Vanhaecke, A. Vantomme, C. Delerue, G. Allan, Z. Hens, Size-dependent optical properties of colloidal PbS quantum dots, ACS Nano 3 (2009) 3023–3030.
[3] O. Gutfleisch, M.A. Willard, E. Brück, C.H. Chen, S.G. Sankar, J.P. Liu, Magnetic materials and devices for the 21st century: stronger, lighter, and more energy efficient, Adv. Mater. 23 (2011) 821–842.
[4] Q. Sun, B. Aguila, J. Perman, A.S. Ivanov, V.S. Bryantsev, L.D. Earl, C.W. Abney, L. Wojtas, S. Ma, Bio-inspired nano-traps for uranium extraction from seawater and recovery from nuclear waste, Nat. Commun. 9 (2018) 1644.
[5] T. Cheisson, E.J. Schelter, Rare earth elements: mendeleev's bane, modern marvels, Science 363 (2019) 489–493.
[6] Y. Yuan, Y. Yang, K.R. Meihaus, S. Zhang, X. Ge, W. Zhang, R. Faller, J.R. Long, G. Zhu, Selective scandium ion capture through coordination templating in a covalent organic framework, Nat. Chem. 15 (2023) 1599–1606.
[7] B. Van de Voorde, B. Bueken, J. Denayer, D. De Vos, Adsorptive separation on metal–organic frameworks in the liquid phase, Chem. Soc. Rev. 43 (2014) 5766–5788.
[8] A. Lee, J.W. Elam, S.B. Darling, Membrane materials for water purification: design, development, and application, Environ. Sci.: Water Res. Technol. 2 (2016) 17–42.
[9] B. Liang, X. He, J. Hou, L. Li, Z. Tang, Membrane separation in organic liquid: technologies, achievements, and opportunities, Adv. Mater. 31 (2019) 1806090.
[10] Z. Tan, S. Chen, X. Peng, L. Zhang, C. Gao, Polyamide membranes with nanoscale Turing structures for water purification, Science 360 (2018) 518–521.
[11] A.W. Mohammad, Y.H. Teow, W.L. Ang, Y.T. Chung, D.L. Oatley-Radcliffe, N. Hilal, Nanofiltration membranes review: recent advances and future prospects, Desalination 356 (2015) 226–254.
[12] P. Sarkar, S. Modak, S. Karan, Ultraselective and highly permeable polyamide nanofilms for ionic and molecular nanofiltration, Adv. Funct. Mater. 31 (2021) 2007054.
[13] J. Zhu, S. Yuan, J. Wang, Y. Zhang, M. Tian, B. Van der Bruggen, Microporous organic polymer-based membranes for ultrafast molecular separations, Prog. Polym. Sci. 110 (2020) 101308.
[14] Z. Jiang, R. Dong, A.M. Evans, N. Biere, M.A. Ebrahim, S. Li, D. Anselmetti, W. R. Dichtel, A.G. Livingston, Aligned macrocycle pores in ultrathin films for accurate molecular sieving, Nature 609 (2022) 58–64.
[15] S. Karan, Z. Jiang, A.G. Livingston, Sub-10 nm polyamide nanofilms with ultrafast solvent transport for molecular separation, Science 348 (2015) 1347–1351.
[16] W.-H. Zhang, M.-J. Yin, Q. Zhao, C.-G. Jin, N. Wang, S. Ji, C.L. Ritt, M. Elimelech, Q.-F. An, Graphene oxide membranes with stable porous structure for ultrafast water transport, Nat. Nanotechnol. 16 (2021) 337–343.
[17] B. Liang, H. Wang, X.H. Shi, B.Y. Shen, X. He, Z.A. Ghazi, N.A. Khan, H. Sin, A. M. Khattak, L.S. Li, Z.Y. Tang, Microporous membranes comprising conjugated polymers with rigid backbones enable ultrafast organic-solvent nanofiltration, Nat. Chem. 10 (2018) 961–967.
[18] Z. Wang, S. Zhang, Y. Chen, Z. Zhang, S. Ma, Covalent organic frameworks for separation applications, Chem. Soc. Rev. 49 (2020) 708–735.
[19] P.J. Waller, F. Gándara, O.M. Yaghi, Chemistry of covalent organic frameworks, Acc. Chem. Res. 48 (2015) 3053–3063.
[20] S.-Y. Ding, W. Wang, Covalent organic frameworks (COFs): from design to applications, Chem. Soc. Rev. 42 (2013) 548–568.
[21] X. Zhang, B. Tu, Z. Cao, M. Fang, G. Zhang, J. Yang, Y. Ying, Z. Sun, J. Hou, Q. Fang, Z. Tang, L. Li, Anomalous mechanical and electrical interplay in a covalent organic framework monolayer membrane, J. Am. Chem. Soc. 145 (2023) 17786–17794.
[22] J. Liu, G. Han, D. Zhao, K. Lu, J. Gao, T.-S. Chung, Self-standing and flexible covalent organic framework (COF) membranes for molecular separation, Sci. Adv. 6 (2020) eabb1110.
[23] X. Li, S. Cai, B. Sun, C. Yang, J. Zhang, Y. Liu, Chemically robust covalent organic frameworks: progress and perspective, Matter 3 (2020) 1507–1540.
[24] L. Cao, I.C. Chen, Z. Li, X. Liu, M. Mubashir, R.A. Nuaimi, Z. Lai, Switchable Na^{+} and K^{+} selectivity in an amino acid functionalized 2D covalent organic framework membrane, Nat. Commun. 13 (2022) 7894.
[25] N. Elmerhi, S. Kumar, M. Abi Jaoude, D. Shetty, Covalent organic framework-derived composite membranes for water treatment, Chem. Asian J. 19 (2024) e202300944.
[26] Q.-W. Meng, X. Zhu, W. Xian, S. Wang, Z. Zhang, L. Zheng, Z. Dai, H. Yin, S. Ma, Q. Sun, Enhancing ion selectivity by tuning solvation abilities of covalent-organic-framework membranes, Proc. Natl. Acad. Sci. U.S.A. 121 (2024) e2316716121.
[27] M.B. Asif, S. Kim, T.S. Nguyen, J. Mahmood, C.T. Yavuz, Covalent organic framework membranes and water treatment, J. Am. Chem. Soc. 146 (2024) 3567–3584.
[28] D.W. Burke, Z. Jiang, A.G. Livingston, W.R. Dichtel, Two-dimensional covalent organic framework membranes for liquid-phase molecular separations: state of the field, common pitfalls, and future opportunities, Adv. Mater. 36 (2024) 2300525.
[29] S. Kandambeth, B.P. Biswal, H.D. Chaudhari, K.C. Rout, H.S. Kunjattu, S. Mitra, S. Karak, A. Das, R. Mukherjee, U.K. Kharul, R. Banerjee, Selective molecular sieving in self-standing porous covalent-organic-framework membranes, Adv. Mater. 29 (2017) 1603945.
[30] K. Dey, M. Pal, K.C. Rout, S. Kunjattu H, A. Das, R. Mukherjee, U.K. Kharul, R. Banerjee, Selective molecular separation by interfacially crystallized covalent organic framework thin films, J. Am. Chem. Soc. 139 (2017) 13083–13091.
[31] H. Wang, Y. Zhai, Y. Li, Y. Cao, B. Shi, R. Li, Z. Zhu, H. Jiang, Z. Guo, M. Wang, L. Chen, Y. Liu, K.-G. Zhou, F. Pan, Z. Jiang, Covalent organic framework membranes for efficient separation of monovalent cations, Nat. Commun. 13 (2022) 7123.
[32] T. Zhu, Y. Kong, B. Lyu, L. Cao, B. Shi, X. Wang, X. Pang, C. Fan, C. Yang, H. Wu, Z. Jiang, 3D covalent organic framework membrane with fast and selective ion transport, Nat. Commun. 14 (2023) 5926.

[33] H.W. Fan, A. Mundstock, A. Feldhoff, A. Knebel, J.H. Gu, H. Meng, J. Caro, Covalent organic framework-covalent organic framework bilayer membranes for highly selective gas separation, J. Am. Chem. Soc. 140 (2018) 10094–10098.
[34] H.W. Fan, M.H. Peng, I. Strauss, A. Mundstock, H. Meng, J. Caro, High-flux vertically aligned 2D covalent organic framework membrane with enhanced hydrogen separation, J. Am. Chem. Soc. 142 (2020) 6872–6877.
[35] S.S. Yuan, X. Li, J.Y. Zhu, G. Zhang, P. Van Puyvelde, B. Van der Bruggen, Covalent organic frameworks for membrane separation, Chem. Soc. Rev. 48 (2019) 2665–2681.
[36] X. Shi, Z. Zhang, C. Yin, X. Zhang, J. Long, Z. Zhang, Y. Wang, Design of three-dimensional covalent organic framework membranes for fast and robust organic solvent nanofiltration, Angew. Chem., Int. Ed. 61 (2022) e202207559.
[37] X.S. Shi, Z. Zhang, S.Y. Fang, J.T. Wang, Y.T. Zhang, Y. Wang, Flexible and robust three-dimensional covalent organic framework membranes for precise separations under extreme conditions, Nano Lett. 21 (2021) 8355–8362.
[38] A.K. Mohammed, A.A. Al Khoori, M.A. Addicoat, S. Varghese, I. Othman, M. A. Jaoude, K. Polychronopoulou, M. Baias, M. Abu Haija, D. Shetty, Solvent-influenced fragmentations in free-standing three-dimensional covalent organic framework membranes for hydrophobicity switching, Angew. Chem., Int. Ed. 61 (2022).
[39] E.R. Nightingale Jr., Phenomenological theory of ion solvation. effective radii of hydrated ions, J. Phys. Chem. 63 (1959) 1381–1387.
[40] Z. Li, H. Li, X. Guan, J. Tang, Y. Yusran, Z. Li, M. Xue, Q. Fang, Y. Yan, V. Valtchev, S. Qiu, Three-dimensional ionic covalent organic frameworks for rapid, reversible, and selective ion exchange, J. Am. Chem. Soc. 139 (2017) 17771–17774.
[41] C. Qian, L. Feng, W.L. Teo, J. Liu, W. Zhou, D. Wang, Y. Zhao, Imine and imine-derived linkages in two-dimensional covalent organic frameworks, Nat. Rev. Chem 6 (2022) 881–898.
[42] K. Vanherck, G. Koeckelberghs, I.F.J. Vankelecom, Crosslinking polyimides for membrane applications: a review, Prog. Polym. Sci. 38 (2013) 874–896.
[43] K. Koner, S. Das, S. Mohata, N.T. Duong, Y. Nishiyama, S. Kandambeth, S. Karak, C. M. Reddy, R. Banerjee, Viscoelastic covalent organic nanotube fabric via macroscopic entanglement, J. Am. Chem. Soc. 144 (2022) 16052–16059.
[44] K. Dey, S. Bhunia, H.S. Sasmal, C.M. Reddy, R. Banerjee, Self-assembly-driven nanomechanics in porous covalent organic framework thin films, J. Am. Chem. Soc. 143 (2021) 955–963.
[45] M.R. Teixeira, M.J. Rosa, M. Nyström, The role of membrane charge on nanofiltration performance, J. Membr. Sci. 265 (2005) 160–166.
[46] B. Sengupta, Q. Dong, R. Khadka, D.K. Behera, R. Yang, J. Liu, J. Jiang, P. Keblinski, G. Belfort, M. Yu, Carbon-doped metal oxide interfacial nanofilms for ultrafast and precise separation of molecules, Science 381 (2023) 1098–1104.
[47] P. Silva, S. Han, A.G. Livingston, Solvent transport in organic solvent nanofiltration membranes, J. Membr. Sci. 262 (2005) 49–59.
[48] T.F. Huang, B.A. Moosa, P. Hoang, J.T. Liu, S. Chisca, G.W. Zhang, M. AlYami, N. M. Khashab, S.P. Nunes, Molecularly-porous ultrathin membranes for highly selective organic solvent nanofiltration, Nat. Commun. 11 (2020) 5882.
[49] G. Székely, J. Bandarra, W. Heggie, B. Sellergren, F.C. Ferreira, Organic solvent nanofiltration: a platform for removal of genotoxins from active pharmaceutical ingredients, J. Membr. Sci. 381 (2011) 21–33.
[50] P. Marchetti, M.F. Jimenez Solomon, G. Szekely, A.G. Livingston, Molecular separation with organic solvent nanofiltration: a critical review, Chem. Rev. 114 (2014) 10735–10806.
[51] V. Balaram, Rare earth elements: a review of applications, occurrence, exploration, analysis, recycling, and environmental impact, Geosci. Front. 10 (2019) 1285–1303.
[52] X.-H. Qi, K.-Z. Du, M.-L. Feng, Y.-J. Gao, X.-Y. Huang, M.G. Kanatzidis, Layered $A_2Sn_3S_7{\cdot}1.25H_2O$ (A = organic cation) as efficient ion-exchanger for rare earth element recovery, J. Am. Chem. Soc. 139 (2017) 4314–4317.
[53] H. Zhang, X. Quan, X. Fan, G. Yi, S. Chen, H. Yu, Y. Chen, Improving ion rejection of conductive nanofiltration membrane through electrically enhanced surface charge density, Environ. Sci. Technol. 53 (2019) 868–877.
[54] Z. Cicek, A.A. Mira, Q. Huang, Process development for the extraction of rare earth elements from an acid mine drainage treatment sludge, Resour. Conserv. Recycl. 198 (2023) 107147.
[55] R.M. Pallares, M. Charrier, S. Tejedor-Sanz, D. Li, P.D. Ashby, C.M. Ajo-Franklin, C. Y. Ralston, R.J. Abergel, Precision engineering of 2D protein layers as chelating biogenic scaffolds for selective recovery of rare-earth elements, J. Am. Chem. Soc. 144 (2022) 854–861.
[56] O. Peer-Haim, I. Shefer, P. Singh, O. Nir, R. Epsztein, The adverse effect of concentration polarization on ion-ion selectivity in nanofiltration, Environ. Sci. Technol. Lett. 10 (2023) 363–371.